EPI International Journal of Engineering
Volume 6, Number 2, August 2023, pp. 62-71
DOI: 10.25042/epi-ije.082023.02

*p*ISSN 2615-5109
*e*ISSN 2621-0541

Rectangular Plate Rebound Vibration Suppression using Double Collision Phenomena

Hiroki Matsumoto[a,*], Kazuhiro Kawakita[b]

[a]Department of Engineering, Mechanical Engineering Research Unit, Muroran Institute of Technology, Hokkaido, Japan.
Email:h_matsu@mmm.muroran-it.ac.jp
[b]Department of Engineering, Mechanical Engineering Research Unit, Muroran Institute of Technology, Hokkaido, Japan.

Abstract

The rectangular plate is a model of the internal mirror of a single lens reflex (SLR) camera. The internal mirror model was a rectangular metal plate rotated along its axis around one side of the rectangle. Rebound vibrations occur when the mirror hits the stopper. A double-collision method was introduced to reduce rebound vibration. The timing of the double collision varies with the amount of rebound vibration. 3-Conpornents Particle Image Velocimetry (3-C PIV) and 3-D motion analysis were used to investigate rebound phenomena. The 3-C PIV measured the rebound vibration velocity of the mirror model surface at the moment of the collision. 3-D motion analysis was used to measure the rebound vibration displacement at the moment of collision. When the rebound vibration was small, the low-velocity region on the surface of the mirror model moved in the longitudinal direction. This indicates that the mirror model underwent wave deformation at the moment of collision. When the timing of the second collision was optimized, the deformation of the mirror model at the moment of collision increased and the rebound amount was suppressed.

Keywords: Vibration;Collision;Rebound;PIV;Flat plate;SLR camera

1. Introduction

Single-lens reflex (SLR) cameras have a moving mirror system. When the shutter release button is pressed, the mirror swings up to the upper side of the camera, and the light passing through the lens moves straight to the shutter curtain. After the image sensor is exposed, the mirror swung down and hit the stopper. At this moment, an impact force is applied to the mirror, and rebound vibration occurs. A mirror-rebound vibration-suppressing mechanism is required to continuously capture the picture.

The collision behavior of objects has been studied for a long time. Examples include an elastic sphere and an elastic half-space [1], an elastic sphere and a large thin elastic plate [2]–[5], a tennis racket and a ball or a bat and a ball [6]–[10], and a circular ring [11], [12].

We studied the phenomenon of mirror rebound. To consider a structure that can suppress rebound vibrations, a collision experiment was performed between a mirror model and stopper model. The rebound vibration is indicated by the rebound angle of the mirror model. Previous studies on the collision behavior of mirror models with a single stopper have considered the rebound angle to vary with stopper position. In the case of the single-stopper model, the rebound angle depends on the stopper position. The stopper position, where the rebound angle is the minimum value, was determined in a previous study [13]. This suppression method is based on the vibration mode of the mirror models [14]. Another suppression method is the two-plate bonded mirror model, which changes the bonding points [15].

In this study, a suppression method for the rebound amount of a mirror model, which is a double-collision model, is proposed. This model has two stoppers located on both sides of the mirror model. The amount of suppression was greater than that in previous methods. In this method, double collision phenomena occur and the rebound angle is reduced. The stopper position was important for reducing the rebound angle.

An examination of the effect of pre-impact vibration on the response to low-velocity impact on a rectangular plate showed that impact damage mitigation can be considered [16]. The effect of pre-elastic waves on the amount of rod bounce has been analytically demonstrated [17]. This suggests that in the case of a large bounce, the relationship between the pre-elastic wave and the elastic wave caused by the collision is important. This suggests that the phenomenon may be explained by a concept similar to that of the double-collision condition in the present study. Therefore, to investigate the mechanism of the change in the amount of bounce due to the double impact on a flat plate, we visualized the behavior of the flat plate during the impact and discussed the effect of the timing of the second impact on the elastic deformation caused by the first impact.

*Corresponding author. Tel.: +81-143-46-5334
Mizumoto-cho 27-1
Muroran-shi, Hokkaido, Japan, 050-8585

The purpose of this study was to determine the optimal stopper position to reduce the rebound angle. We explain the suppression mechanisms through visualization using the 3-Components Particle Image Velocimetry (3-C PIV) method for the double collision phenomena of the mirror model.

2. Experimental Method

2.1. Mirror model

The actual internal mirror has parts in the mirror system, such as a sub-mirror or support frame. To measure the vibration behavior of the mirror model with high precision, a simple scaled-up mirror model was used. The mirror model was made of an aluminum plate with 1 mm thick 60x80mm rectangular plates. The characteristics of the rebound phenomenon were almost the same between the actual-size and scaled-up models [8]. The mirror model shown in Fig. 1 is a scaled-up version. Figure 1 and 2 show the mirror model and the stoppers, respectively. As shown in Fig. 1, M3 bolts were used in the fixture to attach the mirror models to the rotating shaft. The mirror model was rotated by using jigs and shafts. The stainless-steel shaft was 4mm in diameter and was mounted on the main body with ball bearings. In the experiment, a mirror model, supported horizontally by a release, was allowed to fall freely. Two stoppers are placed on either side of the mirror. The right stopper was positioned 45 degrees downward and its position was the origin of the stopper position. The stopper was an aluminum column with a diameter of 5 mm and length of 1 mm in contact with the mirror model. The natural frequency of the stopper structure was very large compared with that of the mirror model. Thus, the stopper structure did not affect the rebound phenomenon in this study. The right stopper position was determined by the distance Y_R and Z_R was fixed at 0 mm. As shown in Figure 2, the origin of the right stopper is the right-side edge of the mirror model. The origin of the left stopper was opposite to that of the mirror model and was at the same height as that of the right stopper. The stopper position was determined by the distances Y_R, Y_L, and Z_L from the model edge, as shown, and Y_R could vary from 0 mm to 40 mm in 2 mm increments. Z_L varied in the negative range. Therefore, the mirror model first collided with the right stopper.

2.2. Experiment setup

The rebound vibration of the mirror model was measured using a laser-displacement meter. Figure 2 shows the measurement position of the laser displacement meter (KEYENCE LK-G80). Figure 3 shows a general view of the experimental setup. Figure 4 shows a right view of the experimental setup and schematic of the mirror model angle. The rebound angle was measured at each stopper position. The measured displacement was converted into a mirror model angle θ. As shown in Fig. 4 b, the mirror model was set at an angle θ = 45 degrees by the release bar. When the release bar moved upward, the mirror model fell freely and hit stoppers. To adjust the start angle of the mirror, a release bar was included, and the release stand at the top of the unit could be adjusted from 0 to 13 mm vertically and horizontally. The stopper adjustment stand (Y-Z stage) at the bottom of the unit could be adjusted from 0 to 40 mm in the Y-axis direction and from -10 to 3 mm in the Z-axis direction from the bottom of the stoppers.

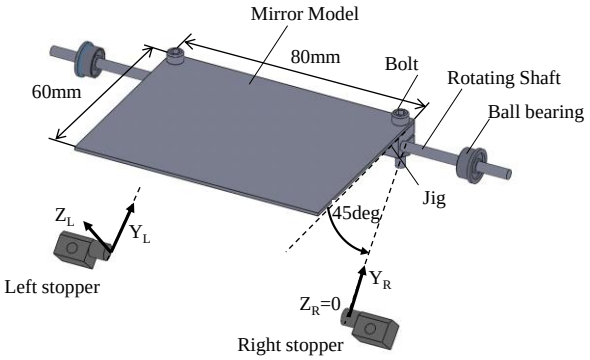

Figure 1. Mirror model and stoppers

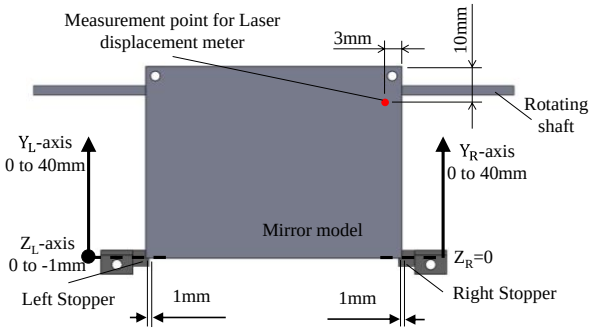

Figure 2. Measurement points and stopper positions

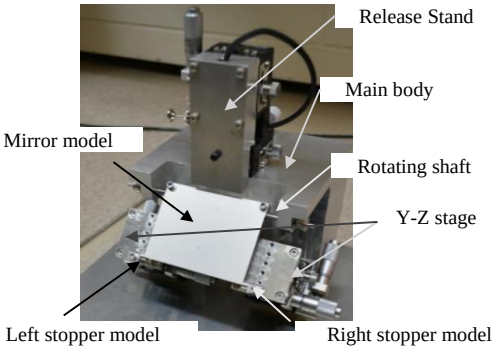

Figure 3. Experimental setup

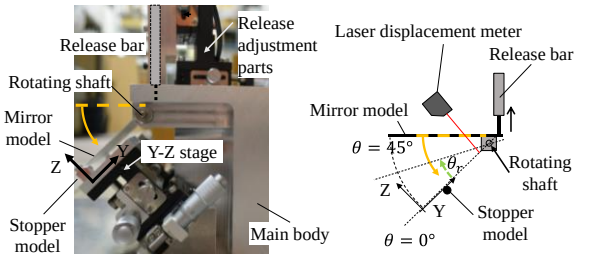

a. Right side view of experiment setup

b. Schematic of the mirror model and the stopper model

Figure 4. Right view of the experimental setup

Figure 5 shows a schematic of the experimental setup of the 3-Components PIV system. A typical stereo particle image velocimetry (PIV) system was used to measure the flow field. Stereo PIV systems use two high-speed cameras to capture images of the particles distributed in a flow field. The spatial motion of the particles was measured by calculating the image correlation of the particle distribution, which was changed for each recorded image. This study used the reflection of the flat plate and mosaic pattern instead of a laser light sheet. This was the originality of the proposed method. Because the plate surface is illuminated, a laser light sheet is not required, and a mosaic pattern instead of particles can be used to measure the behavior of the surface.

The software used for the calculation was Flownizer2D3C from DITECT. This method was used to visualize the transient motion of the mirror model. As shown in Fig. 5, a mosaic pattern was printed on the surface of the mirror model instead of on the particles in the flow. When the mirror hits the stopper, it deforms in the out-of-plane direction, thereby changing the mosaic pattern on the surface of the mirror model captured by the high-speed camera. The change in the mosaic pattern with the deformation of the mirror model was captured using two high-speed cameras, and the moving speed of the mosaic pattern in the 3D space was obtained using the image correlation method. Figure 6 shows the calibration plate used in this method. The displacement of the plate surface was determined by using a dot pattern on the calibration plate. Before the experiment, a calibration plate was placed instead of a mirror model, and the calibration plate dot pattern was captured using two cameras. Two types of images were used to obtain projection functions for each camera. One is the initial position image and the other is the offset image in the Z-direction. Consequently, four projection functions were obtained from the calibration images. The three components of plate displacement require four projection functions. In the software, we set the actual size of the dot, interval of the dot, and offset length. The displacement in the Z-direction is obtained from the mosaic pattern motion of the inspection area. We obtained a mosaic pattern motion in the captured image using the image correlation method in the mirror model measurement.

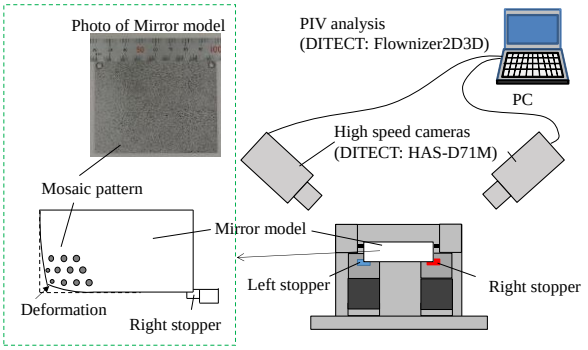

Figure 5. Stereo PIV system

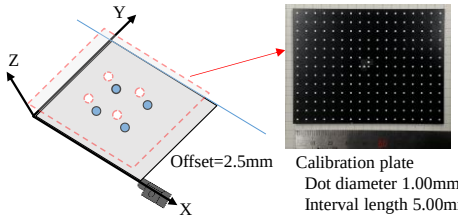

Figure 6. The calibration plate for the stereo camera displacement measurement system

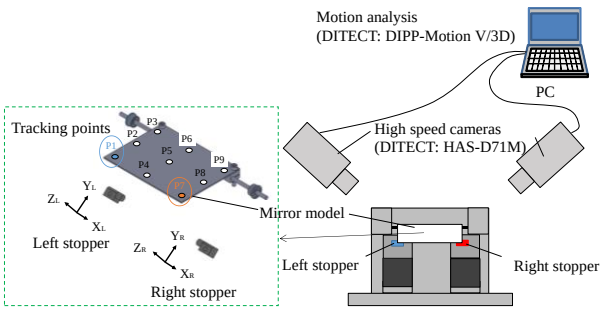

Figure 7. Stereo camera displacement measurement system

Figure 7 shows the displacement measurement system for the mirror model. The displacement of the mirror model during collision was measured using a 3D motion analysis method with two high-speed cameras. Using the obtained images, seven markers on the mirror model were tracked using motion analysis software DIPP-MotionV/3D from DITECT.

3. Experimental Results

3.1. Rebound angle

Figure 8 shows an example of the measured rebound vibration of the mirror model. The vertical displacement of the mirror model was measured using a laser-displacement meter. The vertical displacement was converted into the angle of the mirror model based on the geometric relations. The mirror model falling 45 degrees above the stopper collided with the stopper and rebounded. The maximum rebound angle is defined as the value obtained from the maximum angle recorded at the first impact.

3.2. Rebound angle the mirror model with a single stopper

First, the bounce characteristics of a single stopper were presented. Figure 9 shows the measured maximum rebound angle with a single stopper.

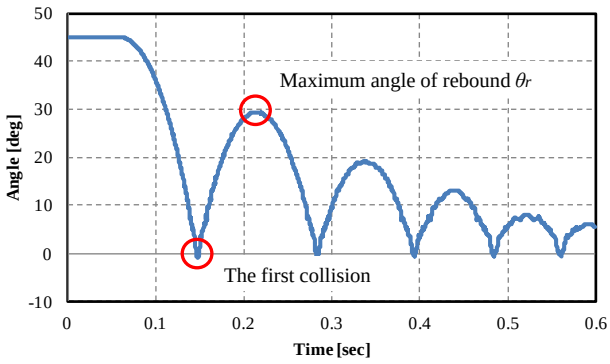

Figure 8. Example of the rebound vibration of the mirror model

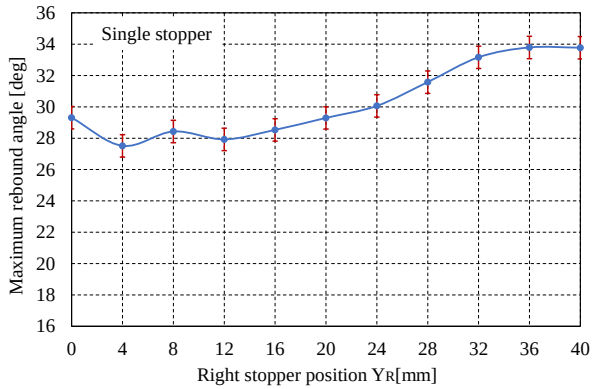

Figure 9. Maximum rebound angle of the mirror model with single-stopper

The graph shows the mean of three experiments, and the error bars represent standard deviations. The position of the stopper on the right side was kept constant at $Z_R = 0$ mm and varied in 4 mm increments from the tip of the mirror model to 40 mm. The maximum rebound angle was measured at each stopper position and plotted. Figure 9 shows that the maximum rebound angle was influenced by the position of the right stopper position. The minimum rebound angle was approximately 27 degrees at $Y_R = 4$ mm.

3.3. Rebound angle of the mirror model with double stoppers

Subsequently, the results for the double-stopper are presented. The right stopper was located at the tip of the mirror model and was fixed at $Y_R = 0$ mm and $Z_R = 0$ mm. The left stopper is located in the Z-direction at $Z_L = 0$ mm, -0.5 mm, and -1 mm. $Z_L = 0$ mm indicates that the left and right stoppers and the mirror model collide simultaneously. A negative Z_L indicates that the mirror model first collides with the right stopper and then with the left stopper.

Figure 10 shows the change in the maximum rebound angle as the position of the left stopper varies during the double collision. When Z_L = -1 mm, the maximum rebound angle was slightly smaller at $Y_L = 0$ mm but was constant with respect to the change in Y_L. The reason for this change is believed to be that the torsional elastic deformation of the mirror model that affects the right stopper produces an elastic deformation of approximately

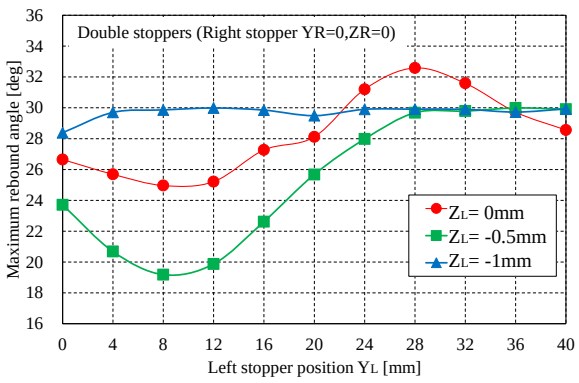

Figure 10. Maximum rebound angle of the mirror model with double stoppers

1 mm at the left tip of the mirror model. When the left stopper is located at the tip of the mirror model, a double collision occurs for $Z_L = 1$ mm, as Y_L increases, the left stopper moves toward the rotation axis of the mirror model, and the elastic deformation of the left end of the mirror model becomes smaller; thus, the left stopper does not collide with the left stopper. Therefore, for $Z_L = -1$ mm and $Y_L = 4$ mm or more, the situation is the same as in the single-stopper case.

The graph for $Z_L = 0$ mm, that is, when both sides collide simultaneously, shows that the maximum rebound angle was smaller than that of the single stopper case for Y_L from 0 to 20 mm, but was larger for Y_L greater than 24 mm. When the two sides of the mirror model collided, a bending deformation occurred. The deformation state is expected to differ depending on the distance between the rotation axis of the mirror model and stopper. When the distance between the rotation axis and the stopper is small, the rebound angle is expected to be larger owing to convex deformation, and when the distance is large, the rebound angle is expected to be smaller owing to concave deformation.

For $Z_L = -0.5$ mm, the rebound angle was smaller than in the single-stopper case over a wide range from $Y_L = 0$ to 24 mm. For $Z_L = -0.5$ mm, the rebound angle was smaller than in the single-stopper case because as Y_L changed, the timing of the collision between the mirror model and the left stopper changed. It can be seen that in the double collision case when the second collision occurs at the appropriate time, the rebound angle is very small. The minimum rebound angle was approximately 19 degrees for $Y_L = 8$ mm and $Z_L = -0.5$ mm, a 40% decrease compared to the single-stopper case.

3.4. Transient response of the mirror model surface velocity

Figures 11 and 12 show the results of the 3-C PIV measurements of the surface velocity of the mirror model colliding with the single-stopper.

Figure 11 shows the results of a single-stopper collision. The stopper positions were $Y_R = 0$ and $Z_R = 0$. The rebound angle is 29.6 degrees. The blue color represents the velocity in the negative direction of the Z-axis, red color represents the velocity in the positive direction, and positive direction of the Z-axis corresponds to the rebound direction. In the case of a single stopper, the collision occurred only once and its duration was set to 0 msec. At the moment of impact, the velocity on the right-side surface of the stopper position is zero, indicating that it is in contact with the stopper. Subsequently, the lower left edge of the mirror model had a negative velocity, which caused elastic deformation of the mirror model with the stopper and rotation as the fulcrum. The deformation continued until 0.875 msec. Subsequently, the lower-left end of the mirror model was found to have a positive velocity. Therefore, the model reached its maximum deformation state at 0.875 msec, after which the lower-left end moved in the positive direction and returned to its original shape. The deformation was restored while maintaining the velocity, and at 2.625 msec, the velocity

of the mirror model near the right stopper became positive, indicating that the stopper and mirror models had separated.

Figure 12 shows the results of a single-stopper collision with a rebound angle of 32.8 degrees. The stopper positions were Y_R = 40 and Z_R = 0. This is the stopper position where the largest rebound angle is measured for all single-stopper conditions. The time from the initial impact to separation from the stopper was 4.125 msec. This indicates that the stopper was in contact with the surface for a longer period than that shown in Fig. 11, where the amount of rebound was smaller. However, the change in the surface velocity distribution of the mirror model was almost the same as that shown in Fig. 11. This indicates that the deformation state of the mirror model was restored after the edge opposite to the stopper was shifted in the negative direction of the Z_R axis. However, in Fig. 12, the position of the stopper is close to the rotation axis of the mirror model. Therefore, after 2.87 msec the region with a positive velocity on the Z_R axis continues to expand along the entire longitudinal direction at the lower edge of the mirror model. This indicates that the range of elastic deformation of the mirror model in the out-of-plane direction is larger than that shown in Fig. 11, and the rebound angle is considered to have increased because of the restoring force of the mirror model.

Figure 13 shows the measurement results of a double stopper, in where the two stoppers collide simultaneously. The coordinates of the left stopper are Y_L = 0 and Z_L = 0, and the coordinates of the right stopper are Y_R = 0 and Z_L = 0. In this case, the left and right stoppers are in the same position relative to the rotation axis; therefore, the mirror model and stopper collided almost simultaneously. In this case, the maximum rebound angle was 25.0 degrees, which was slightly smaller than that in the single-stopper case. The surface velocity distribution of the mirror model after the collision showed that the velocity at the center of the lower edge of the mirror model had a negative component after 0.125 msec, whereas the velocity at both ends in contact with the stopper was zero. This result indicates that the center of the bottom edge of the mirror was elastically deformed in a concave manner. Subsequently, the velocity became almost zero at 0.625 msec, which is expected to indicate that the maximum deformation has occurred. As time passed, the velocity of the center section became positive, and it was found to

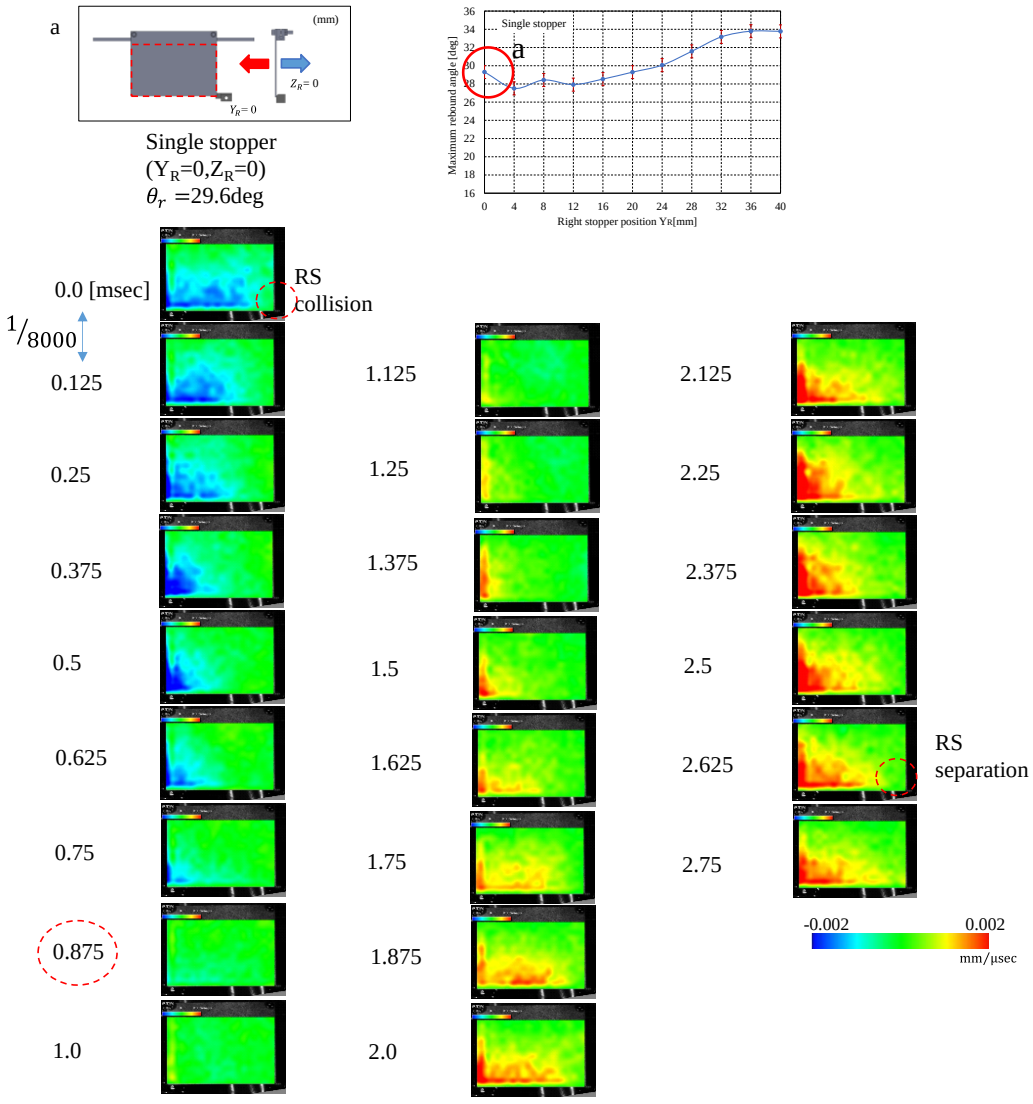

Figure 11. Transient response of mirror model surface velocity measured by PIV. Single stopper (Y_R=0, Z_R=0)

bounce back with the stoppers at both ends as a support. It was found that the model bounced off the stoppers 1.5 msec after the initial collision. After leaving the stoppers, the velocities on both sides of the bottom edge of the mirror model became positive, which was expected to produce an oscillation with a vibration belly at the center. The time from the impact to rebound was shorter than that for a single stopper. This was because the stopper supported the mirror model at two points, resulting in less deformation of the mirror model.

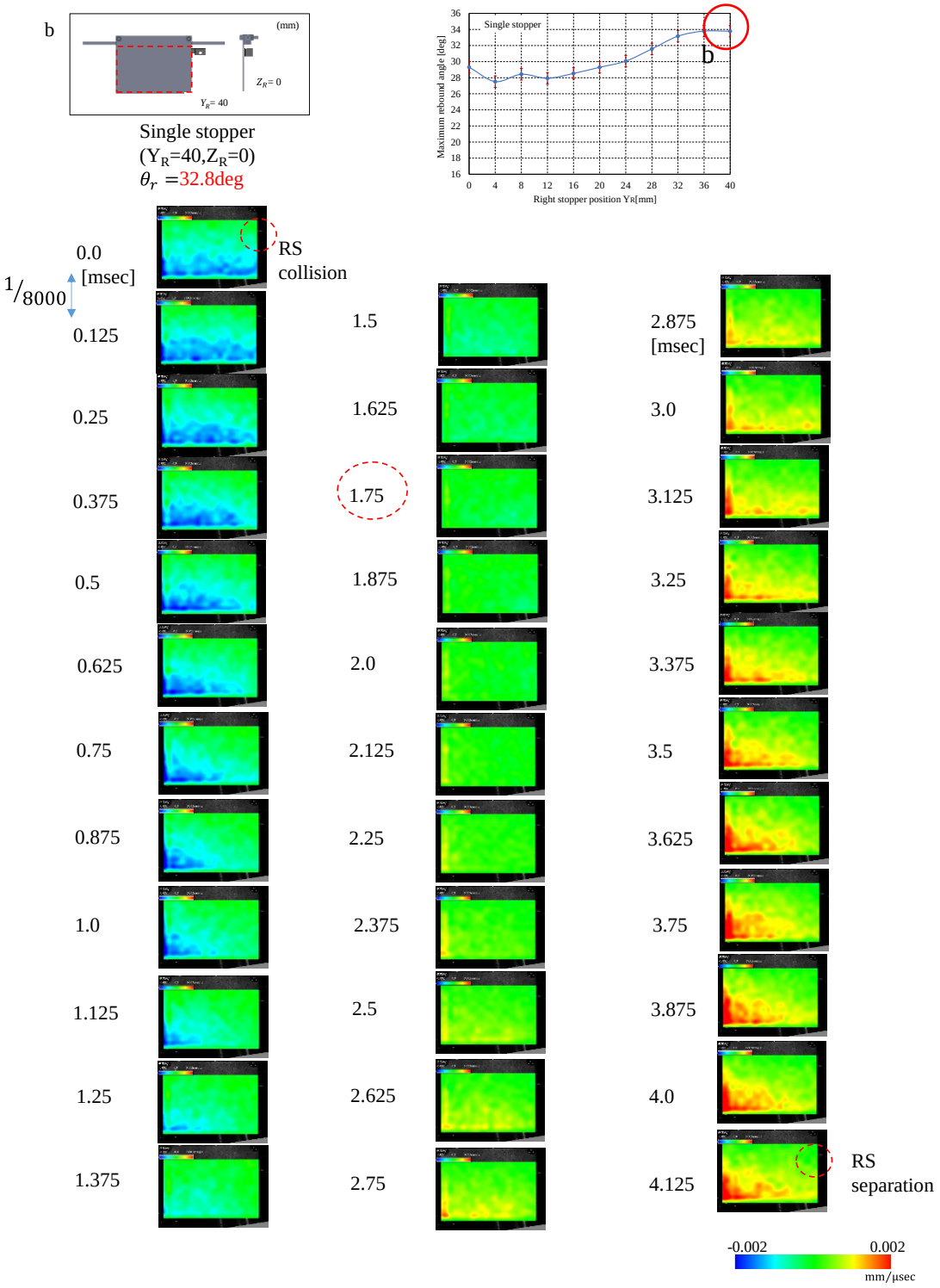

Figure 12. Transient response of mirror model surface velocity measured by PIV. Single stopper (Y_R=40, Z_R=0)

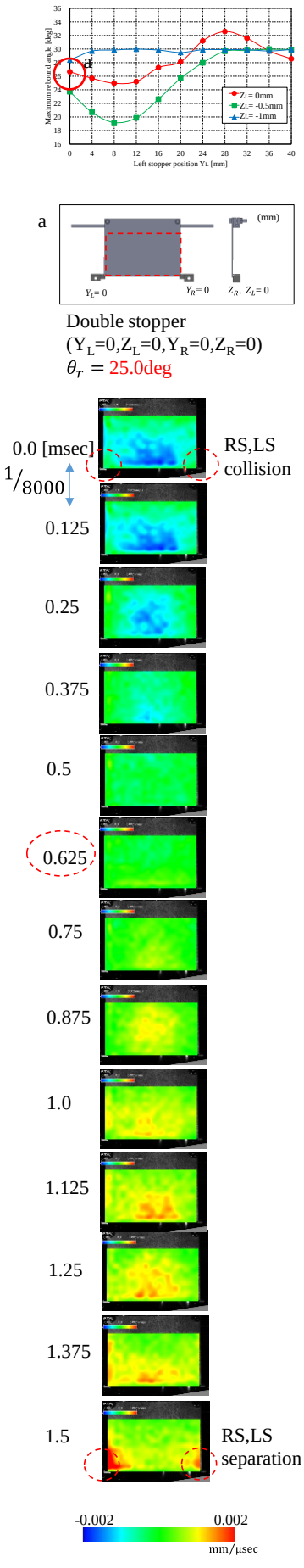

Figure 13. Transient response of the mirror model surface velocity measured by PIV. (a) Double stopper (Y_L=0, Z_L=0, Y_R=0, Z_R=0)

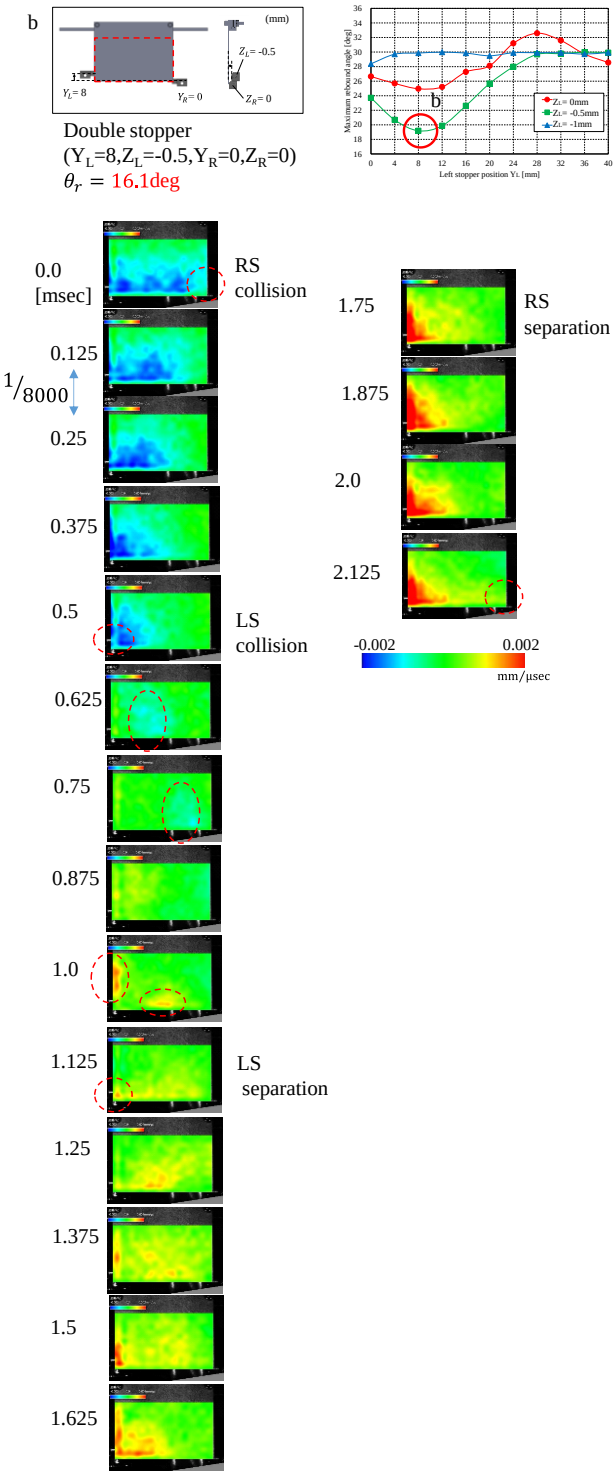

Figure 14. Transient response of the mirror model surface velocity measured by PIV. (b) Double stopper (Y_L=8, Z_L=-0.5, Y_R=0, Z_R=0)

Figure 14 shows the measurement results of the mirror model when the amount of bounce was minimized. The coordinates of the left stopper are Y_L = 0 and Z_L = -0.5, and the coordinates of the right stopper are Y_R = 0 and Z_L = 0. The right stopper was the same as that in Fig. 13, but the position of the left stopper was changed and the time of the second collision with the mirror model was different. The mirror model first collided with the right stopper, and the time was set to 0 msec. After collision with the right stopper, the lower left edge of the mirror model has a negative velocity, indicating that it has been deformed in

the same manner as the single stopper. Subsequently, the mirror model collided with the left stopper. After the second collision at 0.5 msec, the left end of the mirror model had zero velocity, but there was a light blue region near the center of the model, indicating that a negative velocity region was generated. This region moves slightly to the right at 0.625 to 0.75 msec, indicating that the mirror model is deformed in a wave-like manner. In Fig. 13, there is no such shift in the velocity distribution, and the deformation of the mirror model is assumed to be the same as that of the vibration mode at the boundary condition where the model is in contact with the stopper. However, in Fig. 14, the position where the maximum velocity is generated transiently changes from 1 msec to 1.5 msec, producing a more complex deformation and vibration state. This suggests that the second collision occurred before the elastic deformation caused by the first collision was complete, resulting in a more complex deformation and energy consumption. This mechanism resulted in a smaller maximum rebound angle.

Figure 15 shows the maximum rebound measured in the case of double collision. The stopper positions are Y_L = 28 and Z_L = 0 on the left side and Y_R = 0 and Z_R = 0 on the right side. Because the Z-axis heights of the left and right stoppers are the same, we can see that they initially hit the mirror model simultaneously. The tip of the mirror model then elastically deformed in the negative direction of the Z-axis, and at 0.625 msec, the surface velocity reached zero, indicating the maximum deformation state. The elastic deformation of the mirror model then began to recover, with the left side of the mirror model having a greater velocity than the right side. Therefore, the left stopper was the first to be separated from the mirror model at 1.0 msec. Subsequently, the positive velocity distribution at the tip of the mirror model extended along the entire length of the tip of the mirror model, showing the same behavior of increasing the amount of rebound, as shown in Fig. 12. This indicates that a large rebound occurred during the double collision.

3.5. Transient response of the mirror model displacement

Figures 16 - 18 show the transient behavior of the mirror model tip displacement, as measured by 3-D motion analysis.

Figure 16 shows the transient behavior during collision with a single stopper. The model collided with the stopper approximately 2 msec after the start of analysis. The measured velocity of the surface of the mirror model by 3-C PIV corresponds to the 0.0 msec figure in Fig. 11.

Tracking point P1 on the left side of the mirror model showed a negative displacement after the collision, indicating that it had a negative velocity. It is also clear that tracking point P7 on the right side of the mirror model was not displaced and had a velocity of almost zero, which is consistent with the slope of the displacement measurement results from the 3D motion analysis and the measurement results from the 3-C PIV. This confirms the validity of the 3-C PIV measurement for a solid surface. When the mirror model collided with a single stopper, the opposite side of the mirror model was elastically deformed

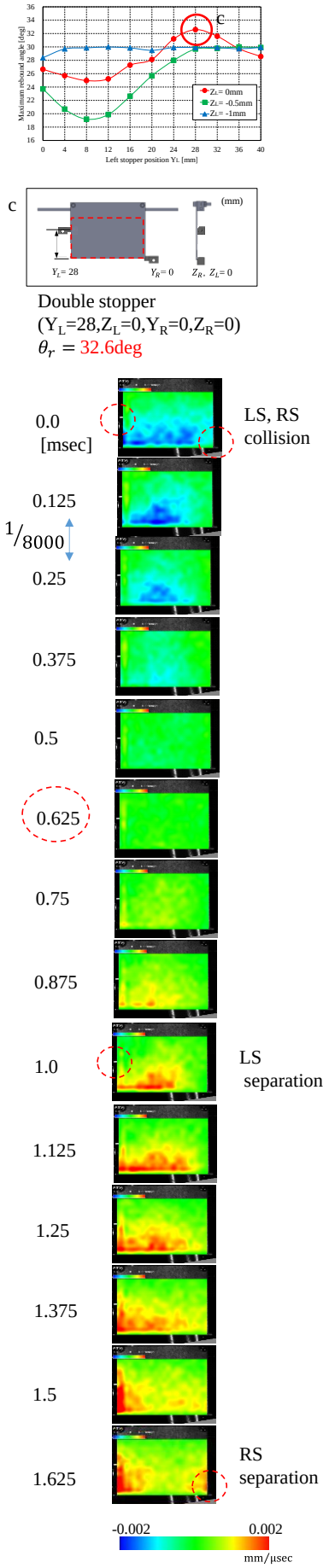

Figure 15. Transient response of the mirror model surface velocity measured by PIV. (c) Double stopper (Y_L=28, Z_L=0, Y_R=0, Z_R=0)

in the negative direction and rebounded because of its restoration. The measurement results in Fig. 16 show that the mirror model after detachment from the stopper vibrated with its tip in the opposite phase after detachment from the right stopper. The left tip had a higher velocity and the right tip had a lower velocity when it detached from the stopper, indicating that torsional vibrations occurred after the model detached from the stopper.

Figure 17 shows the transient behavior of the mirror model tip displacement when the rebound angle was minimized using a double stopper. In this case, the mirror model collided with the right stopper and then with the left stopper at approximately 0.5 msec later. Therefore, the displacement of P1 after 2.5 msec in the graph is limited to 0.5 mm. As shown in the previous section, in contact with the stopper, the mirror model oscillates in a complex manner, and vibrational motion appears in the displacement waveform immediately before the stopper disengages. At the time of disengagement, the positive velocity on the left side was extremely high, and the velocity difference with the right side caused torsional oscillations. In addition, high-frequency oscillations, which are expected to have higher vibration energy, are superimposed. Therefore, positional energy was consumed by the vibration of the mirror model, resulting in a smaller rebound angle.

Figure 18 shows the transient behavior of the mirror model tip displacement when the maximum rebound angle was reached using the double stopper. In this case, the mirror model and stopper collided almost simultaneously because the height of the stoppers were the same. As in the case of collision with a single stopper, the left tip of the mirror model was slightly displaced in the negative direction.

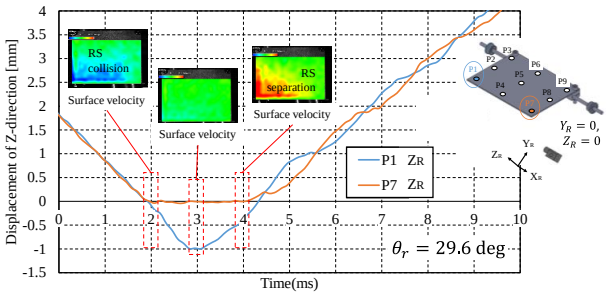

Figure 16. Transient response of the mirror model displacement with the single-stopper (Y_R=0, Z_R=0)

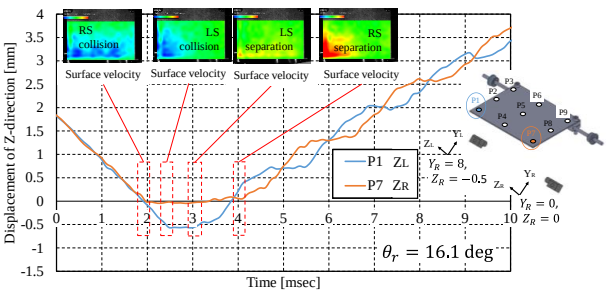

Figure 17. Transient response of the mirror model displacement with the double stoppers (Y_L=8, Z_L=-0.5 and Y_R=0, Z_R=0)

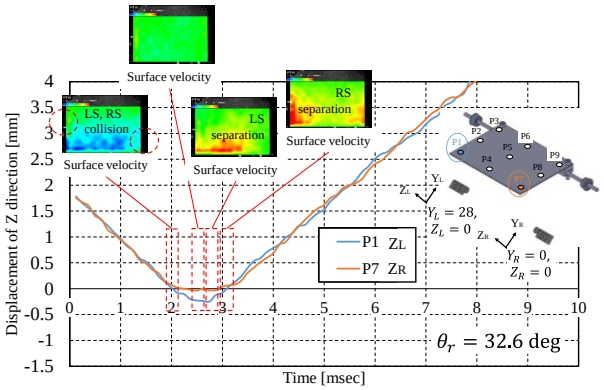

Figure 18. Transient response of the mirror model displacement with the double stoppers (Y_L=28, Z_L=0 and Y_R=0, Z_R=0)

This indicated that the mirror model was elastically deformed. However, in contrast to the single stopper, both sides of the tip of the mirror model rebound at almost the same velocity and without oscillation. Therefore, it can be assumed that the potential energy of the mirror model is not consumed by the vibration of the mirror model and that the amount of rebound is greater.

4. Conclusion

In this study, we investigated a method for suppressing the collision rebound angle of a mirror model by using the double collision phenomenon. The following conclusions were drawn:

(1) The rebound angle of the mirror model varies according to the stopper position and the number of stoppers. The double-stopper case was able to reduce the rebound angle compared to the single-stopper case. The minimum rebound angle was approximately 19 degrees for Y_L = 8 mm and Z_L = -0.5 mm, a 40% decrease compared to the single-stopper case.

(2) From the results of the 3-Component PIV measurement, the transient deformation of the mirror model can be observed from the velocity distribution. After the second collision, the left end of the mirror model had zero velocity, but a negative velocity region was generated in the center region. This region moved slightly to the right, indicating that the mirror model was deformed in a wave-like manner. The second collision causes a more complex deformation than the other stopper positions.

(3) When a double collision occurs during the elastic deformation after the collision, the vibration of the mirror model after the bounce increases, and the vibration of higher frequency components is also generated, resulting in a smaller bounce angle of the mirror model.

References

[1] S. C. Hunter, “Energy Absorbed by Elastic Waves During Impact,” *J. Mech. Phys. Solids*, vol. 5, no. 3, pp. 162–171, 1957.

[2] C. Zener, “The Intrinsic Inelasticity of Large Plates,” *Phys. Rev. Journals*, vol. 59, pp. 669–673, 1941.

[3] P. Mueller, R. Boettcher, A. Russell, M. Truee, and J. Tomas, “A

Novel Approach to Evaluate the Elastic Impact of Spheres on Thin Plates," *Chem. Eng. Sci.*, vol. 138, pp. 689–697, 2015.

[4] P.-K. Tsai, C.-H. Li, C.-C. Lai, K.-J. Huang, and C.-W. Cheng, "Approximation Solution for the Zener Impact Theory," *Mathematics*, vol. 9, p. 2222, 2021.

[5] J. Tengfei *et al.*, "Numerical–Analytical Model for Transient Dynamics of Elastic-Plastic Plate Under Eccentric Low-Velocity Impact," *Appl. Math. Model.*, vol. 70, pp. 490–511, 2019.

[6] Y. Kawazoe, "CAE of Tennis Rackets with Impact Phenomena. Prediction of Racket Response and a View of Restitution in Racket-Ball Impact (in Japanese)," *Trans. Japan Soc. Mech. Eng. Ser. C*, vol. 58, pp. 143–150, 1992.

[7] Y. Kawazoe, "Effect of Racket Frame In-Plane Hoop Vibrations on the Coefficient of Restitution and Energy Losses in Tennis Rackets (in Japanese)," in *The Proceedings of Joint Symposium Symposium on Sports Engineering Symposium on Human Dynamics*, 2006, pp. 130–135.

[8] H. Hata, H. Utsuno, and H. Matsuhisa, "Modal analysis of a metal baseball bat considering the restitution of ball (in Japanese)," in *The Proceedings of Joint Symposium Symposium on Sports Engineering Symposium on Human Dynamics*, 2004, pp. 89–94.

[9] T. Reilly, M. Hughes, and A. Lees, *Science and Racket Sports I*. Taylor & Francis, 2013.

[10] T. Allen, S. Choppin, and D. Knudson, "A Review of Tennis Racket Performance Parameters," *Sport. Eng.*, vol. 19, pp. 1–11, 2016.

[11] R. H. Bao and T. X. Yu, "Impact and Rebound of an Elastic–Plastic Ring on a Rigid Target," *Int. J. Mech. Sci.*, vol. 91, pp. 55–63, 2015.

[12] Y. Wang, Y. L. Yang, S. Wang, Z. Huang, and T. Yu, "Dynamic Behavior of Circular Ring Impinging on Ideal Elastic Wall: Analytical Model and Experimental Validation," *Int. J. Impact Eng.*, vol. 122, pp. 148–160, 2018.

[13] H. Matsumoto and M. Hirashima, "Vibration Behavior and Rebound Angle on the Collision of Mirror Models inside a SLR Camera," *J. Syst. Des. Dyn.*, vol. 7, pp. 393–404, 2013.

[14] H. Matsumoto and M. Hirashima, "Suppression Method for Rebound Amount of the Internal Mirror Model of an SLR Camera," *Mech. Eng. J.*, vol. 2, 2015.

[15] H. Matsumoto, M. Kumagai, and A. Kikuchi, "Rebound Vibration of Two -Plates Bonded Model for an Internal Mirror of SLR Camera," *J. Phys. Conf. Ser.*, vol. 744, 2016.

[16] E. O. Ekpruke, C. V. Ossia, and A. Big-Alabo, "Effect of Pre-Impact Vibrations on the Low-Velocity Impact Response of a Rectangular Plate," *Uniport J. Eng. Sci. Res.*, vol. 5, pp. 18–27, 2020.

[17] B. Lundberg, T. Rastemo, and J. Huo, "Effect of Pre-Impact Waves in an Elastic Rod on Coefficient of Restitution".